Check for updates

Catalytic activity of 1D chains of gold oxide on a stepped gold surface from density functional theory†

Shikun Li, [b] Okikiola Olaniyan, [a] Lenard L. Carroll, [a] Marcus Bäumer [b] and Lyudmila V. Moskaleva *[a]

The rich surface chemistry of gold at the nanoscale has made it an important catalyst for low-temperature applications. Recent studies point to the possible role of self-organized structures formed by chemisorbed O atoms on the surface of gold catalysts for their catalytic activity and/or deactivation. In this study, we investigate the reactivity of a double O chain running along a step on a Au(221) surface with oxygen vacancies as a prototypical model of a 1D surface gold oxide. We compare CO and O_2 adsorption on such a chain with the oxygen-free Au(221) surface model. A systematic study of the reactivity of the double chain with O vacancies was done with respect to the regular Au(221) surface using CO as a probe. The CO oxidation was investigated assuming dissociative and associative mechanisms. Remarkably, O_2 adsorbs stronger on the double oxygen vacancy than on the regular Au(221) surface, and its dissociation barrier reduces significantly from 1.84 eV to 0.87 eV, whereas the CO adsorption energy is similar on these surfaces. Calculations suggest that CO oxidation should occur more efficiently on the double O vacancy than on the regular Au(221) surface due to stronger adsorption of O_2 and a low activation barrier for O_2 + CO surface reaction.

a Department of Chemistry, Faculty of Natural and Agricultural Sciences, University of the Free State, PO Box 339, Bloemfontein 9300, South Africa. E-mail: lyudmila.moskaleva@gmail.com

b Institute of Applied and Physical Chemistry and Center for Environmental Research and Sustainable Technology, University of Bremen, 28359 Bremen, Germany

† Electronic supplementary information (ESI) available: Critical reaction pathways calculated with larger size of the surface unit cell and comparing GGA and meta-GGA functionals. PDOS plots for O adsorption on Au surfaces. Adsorption energies of CO and O_2 computed with various dispersion correction methods. Additional possible reaction paths for O_2 dissociation and for an associative mechanism. See DOI: https://doi.org/10.1039/d2cp03524c

Introduction

Gold nanoparticles and nanoporous gold[1] have attracted significant interest in heterogeneous catalysis as excellent catalytic materials which can be applied for the oxidative esterification of methacrolein and the hydrohalogenation of acetylene reactions in the chemical industry.[2] Nanostructured gold has been reported to exhibit high activity and selectivity for the oxidative coupling and electro-oxidation of alcohols,[3–5] selective hydrogenation of unsaturated hydrocarbons,[6] water-gas shift reaction,[7,8] and especially in the low-temperature oxidation of carbon monoxide.[9–11]

In the 1980s, the groups of Haruta and Hutchings independently discovered that very small gold nanoparticles could be extraordinarily good catalysts. Haruta *et al.*[12,13] demonstrated the catalytic activity of the nanoparticles for low-temperature CO oxidation and Hutchings[14] found them active for hydrochlorination of acetylene to vinyl chloride. Subsequently, the reaction activity and mechanism of CO oxidation by nanostructured gold-based catalysts have been extensively investigated in different experimental and theoretical studies.[15–21] Hu *et al.*[16] suggested a two-step mechanism where CO initially reacts with O_2 to form a CO_2 molecule and an adsorbed O atom which could also quickly bind to CO to form CO_2. Fajín *et al.*[17] suggested a two-step mechanism, first forming a four-atom compound OCOO *via* the direct binding of CO and O_2 followed by a dissociation of the compound into CO_2 and an adsorbed O as a possibly preferable reaction pathway for CO oxidation on the Au(321) surface. Another possible mechanism is that O_2 first dissociates on the gold surface to produce adsorbed atomic O which could directly bind with CO. Although the dissociation of O_2 suffers from a relatively high energy barrier on the gold surfaces,[16,17,22] the dissociation probability of O_2 could be enhanced by modifying the gold catalysts, *e.g.* by alloying.[23,24]

In the above-mentioned mechanisms for CO oxidation, the O_2 molecule plays a prominent role in the reaction activity as either a reactive adsorbed molecular oxygen or as a source of the atomic oxygen from the dissociation step. The activation

This journal is © the Owner Societies 2022

Phys. Chem. Chem. Phys., 2022, **24**, 28853–28863 | 28853

and dissociation of O_2 have also been extensively investigated on the single-crystalline gold surfaces.[24] For example, the low-index gold surface Au(110) was reported to be inert for the chemisorption and dissociative adsorption of the O_2 molecule.[22] Similarly, molecular oxygen will not spontaneously adsorb on a low-index Au(111) surface above 100 K,[25,26] while DFT calculations predict that it should weakly adsorb on a Au(211) surface or a stretched Au(111) surface.[27] Calculations suggested that the steps and tensile strain on the surface should strengthen the O_2 adsorption.[27] On the even-sized subnanometric gold clusters, O_2 was found to chemisorb in two forms, as a superoxo (O_2^-) or peroxo (O_2^{2-}) moiety, *via* an electron transfer from the gold cluster to O_2.[28] Previous computational studies found that O_2 is more reactive for the adsorption and dissociation on the stepped and kinked Au surfaces compared to the flat Au(111) surface, which mainly results from the undercoordinated and hence more reactive Au atoms on the steps.[27,29–31]

Upon a dissociative adsorption of O_2 on a stepped gold surface, the electron-rich O atoms will preferably either occupy the two-fold coordination sites on the step or three-fold fcc sites adjacent to the step.[32] Earlier computational work indicated that the diffusion barrier of O atoms from steps to terrace sites is comparatively high; therefore, most of the dissociated O atoms will probably reside on or close to steps.[33] Therefore, as the number of surface O atoms increases, O atoms may arrange in one- or two-dimensional chain structures. Such chains of O atoms may in general run along or across the steps on a gold surface possibly forming branching structures.[29,34–37] Sun *et al.*[35] addressed the formation of a linear O–Au–O structure on various gold surfaces using Hückel theory and by DFT calculations, finding a significant stabilization of the atomic O adsorption in such structures. In our previous study, we have shown by *ab initio* molecular dynamics (AIMD) simulations that the surface oxygen atoms tend to form a continuous –(Au–O)– chain structure on the step of a Au(321) surface.[38] Scanning tunnelling microscopy (STM) combined with DFT modelling also demonstrated that oxygen atoms could form quasi-ordered oxygen chains at low coverage on a Au(110) surface.[39] Several other computational studies[36,37,40,41] have confirmed the thermodynamic stability of the oxygen chain structures on gold surfaces under specific temperature and pressure conditions.

The pre-adsorbed O atoms on the stepped gold surface have also been reported to facilitate the dissociation of O_2.[37,42,43] Friend *et al.*[42] were able to demonstrate the enhanced dissociation probability of O_2 through the temperature programmed desorption (TPD) on the Au(111) surface pre-covered by atomic O using the electron bombardment of condensed NO_2. In a computational study,[44] AIMD simulations were used to study the adsorption and reaction of CO on the oxygen-covered Au(111) surface, and it was found that the residence time of CO increases, albeit the adsorption probability of CO decreases with the increase in the oxygen coverage.

The nature of the reactive O species on a stepped gold surface has been at the heart of intensive research in heterogeneous catalysis. We expect that linear ("one-dimensional") O chains may be formed on the stepped gold surface when there is a sufficient supply of O atoms,[39] whereas two-dimensional O chains are likely to form in an abundant supply of O atoms (as for example, on Au surfaces with pre-adsorbed O[23,45–48] or in molecular beam experiments[49,50]). O atoms in such 1D and 2D oxide structures are expected to be less reactive compared to individual O atoms, and, therefore, formation and growth of O chains may also occur during ambient oxidation catalysis on Au-based catalysts, such as nanoporous gold. At present, experimental evidence on the chemical nature of surface Au oxide is scarce, but theoretical studies based on *ab initio* thermodynamics predicted "single" (consisting of linear –O–Au–O– units) and "double" (consisting of square shaped –AuO_4– units) O chains along the straight steps of stepped surfaces to be a thermodynamically most stable form of chemisorbed oxygen on Au.[36,41] Such idealized fully saturated O chains are unlikely to be highly reactive (as suggested by their thermodynamic preference over single O atoms). However, in real catalytic systems we expect incomplete chains with O vacancies, which may serve to accommodate adsorbates (such as CO and O_2) and promote reactivity. Reactivity of such incomplete O chains has not been computationally addressed before. In this work, we will investigate the energetics of O atoms chemisorption on the Au(221) surface, our model surface with straight steps. We have calculated the formation energy of different oxygen vacancies in the double chain to determine how the defect prefers to form. We will perform a systematic study to investigate the reactivity of a double O chain with oxygen vacancies and compare the result with the regular Au(221) surface. CO will be used as a probe and the oxidation will be investigated *via* the dissociation and association mechanisms.

Computational models and methods

The Au(221) surface has straight steps and has been chosen as a model surface to investigate the CO oxidation and O_2 dissociation on a double oxygen chain (with O vacancies) which can be formed along the steps of the gold surface (Fig. 1). It is worth noting that the stepped Au surface with preadsorbed self-organized atomic oxygen considered in our work as a model of a gold catalyst is probably only to some extent applicable to gold nanoparticles supported on reducible oxides, such as the ceria-supported gold nanoparticles[51–53] or inverse gold-supported reducible oxide nanoparticles.[54] In such supported catalysts, both the gold nanoparticle and the oxide component are directly involved in the reactivity by helping to activate dioxygen (O_2), and the reaction is believed to occur mainly at the boundary sites between the gold and the oxide components.[52,54–56] However, our models do include a nanostructured oxide component, which is a 1D oxide of gold itself. An enhanced activation of O_2 at the O vacancy sites of a 1D gold oxide found in this work can be related to currently proposed redox mechanisms occurring at the gold-reducible oxide

28854 | *Phys. Chem. Chem. Phys.*, 2022, **24**, 28853–28863
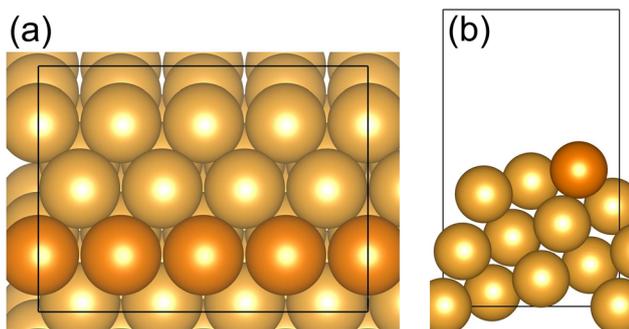
This journal is © the Owner Societies 2022

Fig. 1 (a) Top view (b) side view of the Au(221) surface model. Au atoms at the step edge are indicated by an orange color; the remaining Au atoms are shown in gold.

interface. Therefore, our model is not universal, but it uncovers a new facet of gold surface chemistry which is a tendency to form self-organized nanostructured 1D surface oxide chains that probably contribute to the overall reactivity of the gold-based catalysts. In particular, our model may be relevant to nanoporous gold, which is an unsupported Au catalyst, as well as to Au nanoparticles adsorbed on inert supports.[57]

We used a $p(4 \times 1)$ unit cell of the regular Au(221) surface with a slab thickness of 7.7 Å and 7.2 Å vacuum space separating the slab from its periodic image in the Z direction. Additionally, a larger $p(6 \times 2)$ Au(221) surface model was constructed to elucidate the effect of various sizes of the surface unit cell on the calculated reaction energy diagram (Section I, ESI†). The atoms of the bottom half of the slab were frozen at their bulk geometry while the remaining atoms were allowed to relax without constraints. The double –(Au–O)– chains were constructed along the steps of the surface. A double-chain model was chosen because it corresponds to complete saturation of Au atoms within a chain with O, and hence represents a limiting case of the highest O coverage.

All calculations in this study were carried out with the Vienna *ab initio* simulation package (VASP)[58,59] using the scalar relativistic projector augmented wave (PAW)[60,61] method and plane-wave basis sets. The PAW potentials supplied in VASP (treating Au 5d6s, O 2s2p, and C 2s2p as valence states) have been derived from fully relativistic atomic or ionic reference calculations. VASP treats the valence states in a scalar relativistic approximation, and spin–orbit coupling is neglected. Perdew, Burke, and Ernzerhof (PBE)[62,63] exchange-correlation functional was applied in the calculations. The performance of this functional is discussed in ESI† (Section II) in comparison to a strongly constrained and appropriately normed (SCAN)[64] functional. We have chosen not to include the dispersion correction to avoid overestimation of the adsorption energies of CO and O_2 by the dispersion-corrected PBE functional, but we presented an analysis of how the adsorption energies may change if dispersion correction is included (Fig. S3, ESI†). A $5 \times 5 \times 1$ k-point mesh ($3 \times 3 \times 1$ for test calculations with the $p(6 \times 2)$ model), and the k-point sampling scheme of Monkhorst–Pack[65] grids for the integrations within

the Brillouin zone were used in the calculations. A cut-off energy of 415 eV for the plane-wave basis set and an augmentation charge cut-off energy of 645 eV were adopted. In the calculations, we used Methfessel–Paxton order 1 smearing scheme[66] with a smearing parameter of 0.05 eV. Spin polarization calculations were carried out for all systems containing molecular oxygen and related reaction intermediates and transition states. The relaxation of the surfaces (with the conjugate gradient method) was performed until the force acting on each atom was less than 0.02 eV Å^{-1}, while the energy was converged with a tolerance of 10^{-6} eV. The minimum energy reaction paths were determined by an improved method of the conventional nudged elastic band method (NEB),[67] the climbing-image nudged elastic band method (ci-NEB),[68] and the transition state structures were further refined by the dimer[69] method. The reaction energy and activation barriers were calculated as the difference of the electronic energies of the reactant, product and transition state rather than the Gibbs free energies, because a calculation of vibrational frequencies for many elementary reaction steps considered in this work would be too time-consuming but not necessarily improving the accuracy given the qualitative nature of DFT relative energies. For surface reactions, the thermal corrections and change in entropy are usually small, whereas the entropy term does become significant for the adsorption of CO and O_2 due to a loss of translational entropy (we estimate this entropy loss, $T\Delta S$, to be up to 0.2 eV per molecule at 300 K, assuming mobile adsorbates). We need to keep this in mind when discussing the adsorption energies of CO and O_2 on gold.

Results and discussion

1 Oxygen chain structure on a Au(221) surface

1.1 The formation of an oxygen chain structure. In our previous report,[38] we demonstrated that two or more O atoms adsorbed on the Au(321) surface prefer to form a single-chain structure. Similarly in this study, to investigate the O_2 dissociation and CO oxidation on the Au(221) surface with adsorbed oxygen atoms, we started by calculating the energetics of adsorption geometries of O atoms on the Au(221) surface. The results are shown in Fig. 2. An individual O atom prefers to adsorb at a 3-fold fcc site near the step edge with the adsorption energy (per O atom relative to $1/2 O_2$ molecule) of -0.27 eV (Fig. 2(a)). Two O atoms form a linear –O–Au–O– chain with the Au atom at the step edge of the surface, and the adsorption energy per O atom is -0.29 eV (Fig. 2(b)). As the number of O atoms increases, the adsorption strength increases responsively until a threshold value of 4 O atoms, which corresponds to an adsorption energy per O atom of -0.31 eV, (Fig. 2(c) and (d)). The 4 O atoms formed an infinite –(Au–O)– chain structure along the step edge. We previously found similar stabilization for –(Au–O)– chain structures formed on Au(321) and Au(310) and explained it by the formation of strongly directional Au–O bonds with stronger binding within the chain than between the chain and the underlying
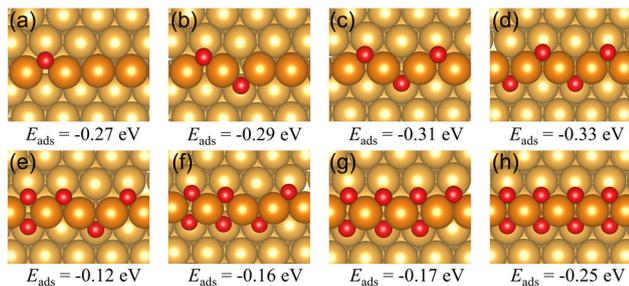
Fig. 2 The adsorption energies (eV) per O atom and the corresponding geometries for various numbers (1–8) of oxygen atoms separately shown in (a–h) in a $p(4 \times 1)$ unit cell on a Au(221) surface. Au atoms at the step edge are indicated by an orange color; the remaining Au atoms are shown in gold. O atoms are shown in red.

Au substrate.[29,37] By increasing the number of the adsorbed O atoms further from 4 to 7, a second chain begins to form in the opposite direction to the initial oxygen chain, and collectively the O atoms appear as a double chain with oxygen vacancies. Consequently, although still exothermic, the adsorption strength of the new chain (per O atom) is less than the single chain due to the growing electrostatic repulsion among the O atoms with the coverage. For instance, the adsorption energy per O atom for 5, 6, and 7 O atoms is -0.12, -0.16, and -0.17 eV, respectively (see Fig. 2(e)–(g)), which is weaker than that of a single oxygen atom adsorbed at the favorable site on the Au(221) surface. However, a perfect double –(Au–O)– chain is formed when the number of O atoms reaches 8 with the adsorption energy of -0.25 eV per O atom (Fig. 2(h)). This value of the adsorption energy is very close to that of one or two oxygen atoms adsorbed on the step (Fig. 2(a) and (b)). We could infer that the strong directional bonding interaction within the –(Au–O)– chain enhances the stability of the chain despite the increasing repulsion among the O atoms. We further compared the projected density of states (PDOS) onto O2s, O2p and Au5d orbitals for several Au(221) surfaces with different types of O adsorption (see Fig. S4, ESI†). When one O atom binds on the Au(221) surface, an orbital overlap between the O2p and Au5d states results in two rather broad resonances near the top and near the bottom of the Au5d band (Fig. S4(b), ESI†). The antibonding states near the top of it are largely occupied preventing a strong covalent bonding. With the formation of a –(Au–O)– chain, the Au5d band widens (this is attributed to the increased coordination of Au atoms) and a new peak appears at the bottom of the Au5d band (Fig. S4(c), ESI†), which shows an enhanced hybridization with the bonding states of the O2p band, contributing to the stronger adsorption of O atoms in the –(Au–O)– structures. For the Au(221) surface with a double O chain, we observed further broadened Au5d and O2p bands (Fig. S4(d), ESI†), where a distinct bonding O2p state at the bottom of the Au5d band and the partially unoccupied anti-bonding state at the top of it indicate stronger Au–O bonding in comparison to the surface adsorbing only one O atom per unit cell. However, a high coverage and high density of O atoms on the step edge within a double O chain also

causes some repulsion and slightly lifts up O atoms, as reflected in the elongated average bond length between the O atoms of the chain and Au atoms on the terrace (~ 0.08 Å), which may be one of the explanations of its lower thermodynamic stability than that of the surface with a single O chain. Therefore, the double chain can be considered a thermodynamically stable form of adsorbed oxygen on the Au(221) surface at high O coverage, *i.e.* when there is an abundant supply of atomic oxygen and sufficient time is allowed for the formation of such oxygen assembly.

1.2 The formation of oxygen vacancies. When there are one or two closely located oxygen defects on a double chain, which could arise from an insufficient supply of oxygen atoms on the Au(221) surface or could form during a reaction with a surface species that can be oxidized, such as CO, oxygen vacancies within a chain could act as active sites for subsequent adsorption of O_2 and CO. We investigated two different types of O defects, single and double oxygen vacancies, as shown in Fig. 3. For a single oxygen vacancy, the formation energy is 0.81 eV, which is almost equal to half of the formation energy of a double O atom vacancy (see Fig. 3). As for the double vacancies, the defects can have different arrangements. Here, we considered two different arrangements for the vacancies. In one of them, the two vacant O sites are adjacent, while in the other they are separated, as shown in Fig. 3(b) and (c). The formation energy of the two adjacent vacancies is less than that of the separated vacancies by 0.16 eV (see Fig. 3(b) and (c)). As a result, it would be easier to form than the separated O vacancies. Therefore, the adjacent vacancies will be selected as the active site for the adsorption and activation of CO and O_2 in our calculations.

2 The adsorption of CO and O_2

2.1 The adsorption of CO. We also investigated the adsorption of a CO molecule on the regular Au(221) surface and on the double chain with oxygen vacancies. The results are shown in Fig. 4. The HOMO of CO is a nonbonding 5σ orbital largely centered on the carbon atom. According to a well-known Blyholder model,[70] CO binds to the metal site through this non-bonding orbital, while at the same time the metal back-donates electrons into the $2\pi^*$ level of CO. The first contribution is dominant explaining why the CO molecule prefers to
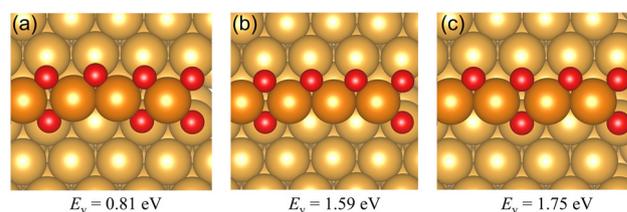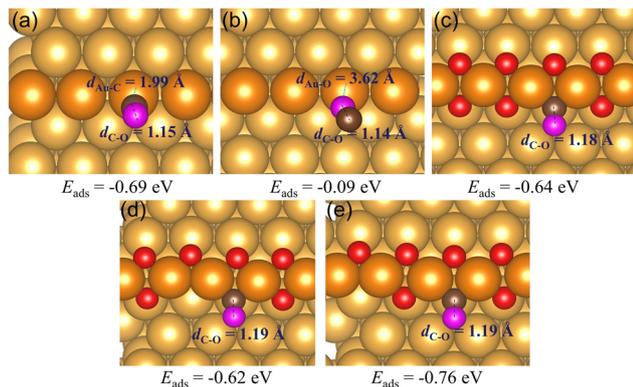

Fig. 3 The oxygen vacancy formation energies and the corresponding geometries of the Au(221) surface having (a) one oxygen vacancy, (b) two adjacent oxygen vacancies, (c) two separate oxygen vacancies. The oxygen vacancy formation energies on the chain structure with two vacancies indicate the total energy required to form two vacancies rather than the average energy per vacancy. Color coding is the same as in Fig. 2.

28856 | *Phys. Chem. Chem. Phys.*, 2022, **24**, 28853–28863

This journal is © the Owner Societies 2022

Fig. 4 The adsorption energies and the corresponding geometries of CO adsorbed on the regular Au(221) surfaces (a) the carbon end, (b) the oxygen end, and on single and double O vacancies of the double oxygen chain with (c) the single vacancy, (d) the adjacent vacancies, or (e) the separate vacancies *via* the carbon end. The C–O bond lengths and selected Au–O/C bond lengths are indicated. Au atoms at the step edge are indicated by an orange color; the remaining Au atoms are shown in gold. O atoms of the chain structure are shown in red, while O and C atoms of the CO molecule are shown in pink and black, respectively.

Fig. 5 (a) The reaction energy diagram and (b) the corresponding geometries of CO* reacting with the oxygen atom of a double chain on a Au(221) surface. Selected bond lengths are listed in the table embedded in panel (a). Color coding is the same as in Fig. 4.

adsorb *via* its carbon end. This is consistent with our calculated values of the adsorption energy of CO, −0.09 eV through the O end and −0.69 eV *via* the C end on the regular Au(221) surface (see Fig. 4(a) and (b)). Similarly, the adsorption energies of CO through the C end on the double chain with one and two adjacent oxygen vacancies are −0.64 and −0.62 eV, respectively (as shown in Fig. 4(c) and (d)). Moreover, we found that the adsorption strength is increased to −0.76 eV when CO is adsorbed on the double chain with two separate vacancies (see Fig. 4(e)). However, in the case of the double chain with oxygen vacancies, the C–O bond length is elongated by 0.04 Å relative to CO adsorption on the regular Au(221), suggesting a stronger π back-donation from Au to the π* of CO. This is consistent with a more covalent (directional) nature of the bonding within a chain and effective low coordination of Au atoms within a chain.

When there is an abundant supply of O atoms, we expect the formation of double oxygen chains along the straight steps on the Au(221) surface. Due to the oxygen-rich nature of this surface oxide, it would be interesting to investigate its ability to oxidize CO and form O vacancies. We consider a process in which one of the O atoms of the chain reacts with the adsorbed CO* molecule (where * denotes the adsorbed state) to form a CO_2* molecule. Consequently, we conducted a ci-NEB calculation with the dimer method to optimize the transition state to search for the likely reaction path (see Fig. 5). The results show that the CO* molecule initially adsorbed at a terrace site moves closer to one of the O atoms of a chain forming a bent CO_2* intermediate through a relatively small barrier of 0.19 eV. The bond length of CO*, $d_{C3–O1}$, reduces from 2.70 Å to 1.37 Å. This bent CO_2* geometry is consistent with the anionic CO_2^- species,[71] which is metastable and easily gives away its extra electron becoming a linear CO_2 with the C–O bond lengths of 1.18 Å through almost zero barrier height. CO_2 has a negligibly
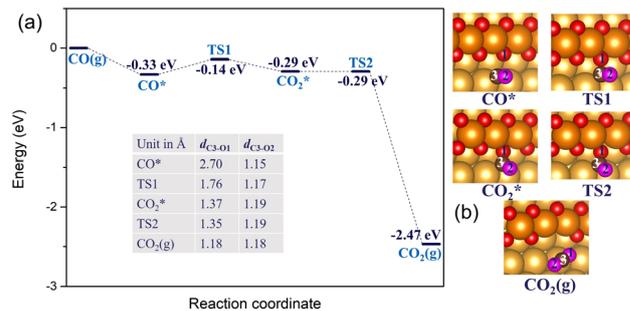
low binding energy on Au; hence, in the final state it is desorbed from the surface. The whole reaction of CO oxidation by the oxygen atom of the double chain releases 2.14 eV exothermically. Thus, such a reaction is expected to be facile. Its rate will be limited by a relatively weak adsorption of CO at flat terrace sites, with the adsorption energy in the range of −0.3 to −0.2 eV (compared to −0.6 eV at low-coordinated Au atoms of a step, which are not available if steps are covered by oxygen).

2.2 The adsorption of O_2. Before we investigate the dissociation of molecular oxygen, it is pertinent to calculate the adsorption energies of molecular oxygen on the regular Au(221) surface and on the double oxygen chain with vacancies formed at a step edge of Au(221). The results are shown in Fig. 6. Molecular oxygen was adsorbed vertically and horizontally to determine the preferred adsorption geometry on the surfaces in question. Our result shows that O_2 prefers to adsorb horizontally on the Au(221) surface regardless of the presence of the O chain. The adsorption energies for the horizontal and vertical binding of O_2 on the regular Au(221) surface are −0.22 and
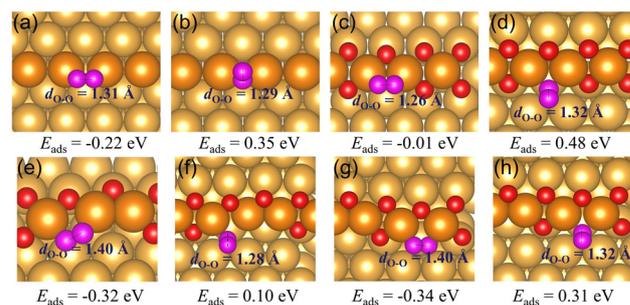

Fig. 6 The adsorption energies and the corresponding geometries of O_2 on various Au(221) surfaces (a) horizontally and (b) vertically adsorbed on a regular Au(221) surface, (c) horizontally and (d) vertically adsorbed on a double oxygen chain with the single vacancy, (e) horizontally and (f) vertically adsorbed on a chain with adjacent vacancies, (g) horizontally and (h) vertically adsorbed on a chain with separate vacancies. The O–O bond lengths of O_2* molecule are indicated. Au atoms at the step edge are indicated by an orange color; the remaining Au atoms are shown in gold color. O atoms of the chain structure are shown in red, while the O atoms of the O_2* molecule are shown in pink.

This journal is © the Owner Societies 2022

Phys. Chem. Chem. Phys., 2022, **24**, 28853–28863 | **28857**

0.35 eV, respectively (see Fig. 6(a) and (b)), while -0.01 and 0.48 eV (Fig. 6(c) and (d)) correspond to the horizontal and vertical adsorption on the surface with a single oxygen vacancy. Moreover, for the surface with two oxygen vacancies, the pairs -0.32 and 0.10 eV and -0.34 and 0.31 eV correspond to the horizontal and vertical O_2 adsorption energies on the surfaces with two adjacent and separate oxygen vacancies, respectively (see Fig. 6(e)–(h)). A much stronger horizontal adsorption of O_2 on double oxygen vacancies compared to a single vacancy can be attributed to additional space available at the adsorption site and a higher flexibility of a chain with removed two O atoms compared to a relatively limited space and flexibility of a single oxygen vacancy site. On the surface with two separate oxygen vacancies, the horizontal adsorption of O_2 is accompanied by a notable distortion of the chain structure. Molecular oxygen is said to be activated if, upon adsorption on a surface, the bond length is significantly enlarged relative to the bond length (1.23 Å) in the gas phase. Our calculations show that the bond length of activated O_2 is 1.40 Å, typical for a peroxo O_2^{2-} species with a zero spin magnetic moment on the surfaces with exothermic adsorption (structures (e) and (g) of Fig. 6), whereas a partially-activated O_2 with a shorter bond length (~ 1.3 Å) shows the spin magnetic moment of approximately 1 which is either evenly distributed over two O atoms (structures (a) and (c) of Fig. 6), or remains mainly localized on the O atom far from the surface (structures (b), (d), (f) and (h) of Fig. 6).

3 The reaction between CO and O_2

In the previous sections, we have demonstrated that the adsorption strength of individually adsorbed O_2^* and CO^* become enhanced on a double O chain with oxygen vacancies formed on a Au(221) surface. Hence, it becomes necessary to explore the reactivity of O_2^* and CO^* adsorbed at O vacancy sites of a chain. The two mechanisms that are considered in this study are dissociation and association mechanisms. In the dissociation mechanism, O_2^* is first activated through its adsorption at an O double vacancy site where it dissociates to form an adsorbed atomic O^*, which could then react with CO^* to form CO_2^* (see eqn (1)). However, in the association mechanism, O_2^* binds directly to CO^* to form a transient $OCOO^*$ intermediate which would then decompose to CO_2^* and an adsorbed O^* atom as outlined in eqn (2). In our previous study of CO oxidation on Au(321), we have theoretically predicted that the associative mechanism should be much faster than the dissociative one at the experimentally relevant conditions, due to a too high dissociation barrier of O_2^* (~ 1 eV).[72]

$$O_2^* \rightarrow O^* + O^* \overset{+CO^*}{\rightarrow} CO_2 \tag{1}$$

$$CO^* + O_2^* \rightarrow OCOO^* \rightarrow CO_2 + O^* \tag{2}$$
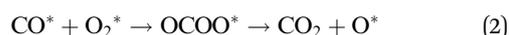
3.1 Dissociation mechanism. In the dissociation mechanism, O_2 is first adsorbed on the surface, then decomposes to form adsorbed O^* atoms. We compare the dissociation of O_2^* on the regular Au(221) surface with the dissociation of O_2^* adsorbed at a double chain with two adjacent oxygen vacancies.
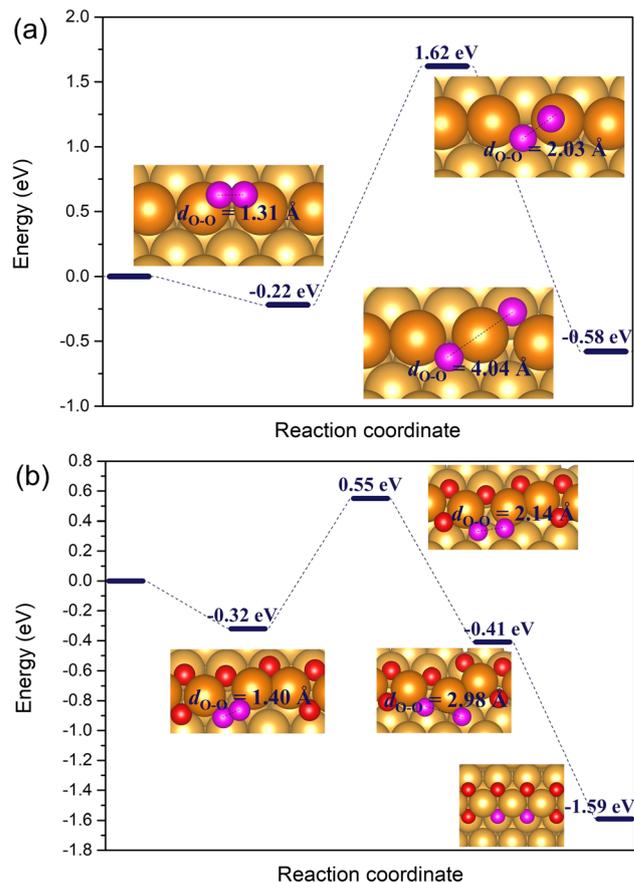

Fig. 7 The reaction energy diagram for the dissociation of O_2^* horizontally adsorbed on (a) the regular Au(221) surface, and (b) the double chain with two adjacent vacancies on the Au(221) surface. The geometries and the O–O bond lengths of O_2^* are given in the insets. Color coding is same as in Fig. 6.

The reaction profiles for O_2^* dissociation are shown in Fig. 7. On the regular Au(221) surface, the adsorption energy of horizontally adsorbed O_2^* is -0.22 eV, while the activation barrier for O_2^* dissociation is as high as 1.84 eV. In the transition state the O–O bond length is elongated to 2.03 Å (from 1.31 Å in the initial state). The dissociation process is slightly exothermic corresponding to a release of 0.36 eV. As for the double chain with two adjacent oxygen vacancies, the adsorption energy of the horizontally adsorbed O_2^* at a vacancy is -0.32 eV, while the barrier height required to stretch the bond length from 1.40 Å in the initial state to 2.14 Å in the TS, is equal to 0.87 eV, about half of the value on the regular Au(221) surface (see Fig. 7(b)). We attribute this barrier lowering to an electron transfer from the vacancy to the antibonding π^* orbital of O_2, in the initial state, which helped to activate O_2^*. The two separate O^* atoms in the final state tend to compensate for the missing O atoms at the vacant sites and form a distorted double chain. We termed it a distorted double chain since one of the complimentary oxygen atoms is distant from the chain and consequently leaves a vacancy in the chain. If the distorted double chain relaxes to an ideal undistorted chain, the energy drops down by a further 1.18 eV. Furthermore, although not the

most favorable adsorption geometry as demonstrated in section 2.2, we also studied O_2* dissociation where one O atom is located at the vacancy of the double chain while the other O atom binds to a Au atom on the terrace (see Fig. S5(a), ESI†). The endothermic adsorption reaches up to 0.41 eV, while the dissociation barrier is 0.32 eV, which is lower than that for the dissociation *via* the horizontal adsorption of O_2. The dissociation process is exothermic and is accompanied by a release of 0.55 eV. The initial geometry of O_2* horizontally adsorbed on the O chain with two separate vacancies shown in Fig. 6(g) was also used to elucidate another possible path for O_2* dissociation. The dissociation barrier of 0.83 eV is close to that of O_2* horizontally adsorbed on the adjacent vacancies, while the dissociation process is endothermic with the reaction energy of 0.76 eV (Fig. S5(b), ESI†).

After the dissociation of O_2*, O vacancies get replenished. A fully saturated or incomplete chain can react with a CO adsorbed at a terrace site, as illustrated in Fig. 5, or, upon formation of one or more O vacancies, CO could adsorb at a vacancy site (as shown in Fig. 4(c) and (d)). A CO molecule adsorbed at a vacancy of a chain is unlikely to react with an O atom of a chain. Such a reaction is found to have a very high barrier of about 1 eV. But it could react with an external individual O* atom adsorbed near a chain, as shown in Fig. 8 below.

Starting with a double chain with a single oxygen vacancy and an adsorbed O* atom located at an fcc-terrace site, we adsorbed CO* at the O vacancy site, and then conducted a NEB

calculation to search for the transition states for the pathway. The reaction profile and the adsorption geometries are shown in Fig. 8. The initial adsorption energy of CO* at the vacancy site is −0.56 eV and later the overall relative energy is lowered to −0.60 eV after the migration of the adsorbed O* atom from an fcc site (labeled as fcc1 in Fig. 8(b)) to an hcp site *via* a barrier height of 0.19 eV. The migration of the O* atom continues as it moves to a new fcc site (labeled as fcc2 in Fig. 8(b)), closer to the adsorbed CO* overcoming an activation barrier of 0.08 eV. Finally, the O* binds with CO* *via* a very low barrier of only 0.02 eV to form CO_2 which then desorbs irreversibly from the surface. Note that the highest barrier along the reaction pathway is for the diffusion of O*, and not the CO_2 formation. The reaction is exothermic and 2.89 eV energy is dispensed in the process. All through the reaction steps, the C3–O2 bond length ($d_{C3–O2}$, 1.18 Å) remains constant, while the distance between C3 and O1 ($d_{C3–O1}$) decreases from 3.95 to 1.18 Å.

To summarize, in the dissociation mechanism, the dissociation of O_2* is the rate-limiting step for the CO oxidation reaction. While the activation barrier for O_2* dissociation on the regular Au(221) is 1.84 eV, the barrier is significantly reduced to 0.87 eV on the double chain with two adjacent oxygen vacancies. CO* adsorbed at a vacancy site can easily react with an O* atom at a nearby terrace site with an almost zero barrier.

3.2 Association mechanism

3.2.1 Regular Au(221) surface. In the association mechanism, O_2* directly binds to the co-adsorbed CO*, forming a metastable OCOO* intermediate. In the next step, OCOO* breaks down to CO_2* and an adsorbed atomic O*. We studied this mechanism on Au(221) with the O chain and on a regular Au(221) surface. On the regular Au(221) surface, the bimolecular co-adsorption of CO and O_2 releases 0.85 eV, with O_2* adsorbing horizontally on a bridge site and CO* vertically on a top site (Fig. 9). CO* would then combine with O_2* to form OCOO* transient intermediate *via* a barrier of 0.14 eV. In the process, the O_2* molecule is activated by elongating its bond length by 0.13 Å while the distance ($d_{C4–O2}$) between the O_2* and CO* decreases from 3.62 Å to 1.37 Å. The formation of the OCOO* intermediate is an exothermic process releasing 0.23 eV energy. Finally, the intermediate dissociates through a barrier of 0.33 eV to CO_2* and the adsorbed O* atom on the surface. Comparing the rate-limiting step in the dissociation and the association mechanisms on the regular Au(221) for CO oxidation, we found the barrier height for the latter to be significantly less than the former by 1.51 eV. Thus, this finding shows that the association mechanism would be more efficient on the regular Au(221) surface. Although the activation energy of CO oxidation is computed to be relatively low on the regular Au(221) surface, the reactivity of extended gold surfaces for CO oxidation is still limited in reality owing to the low concentration and transient time of the adsorbed species (O_2* or CO*) arising from the weak binding strength of O_2 on pure Au, which however may be increased by introducing Ag in nanoporous gold.[73,74] Also, a collision frequency with the surface for an O_2 molecule trapped inside a nanopore presumably increases compared
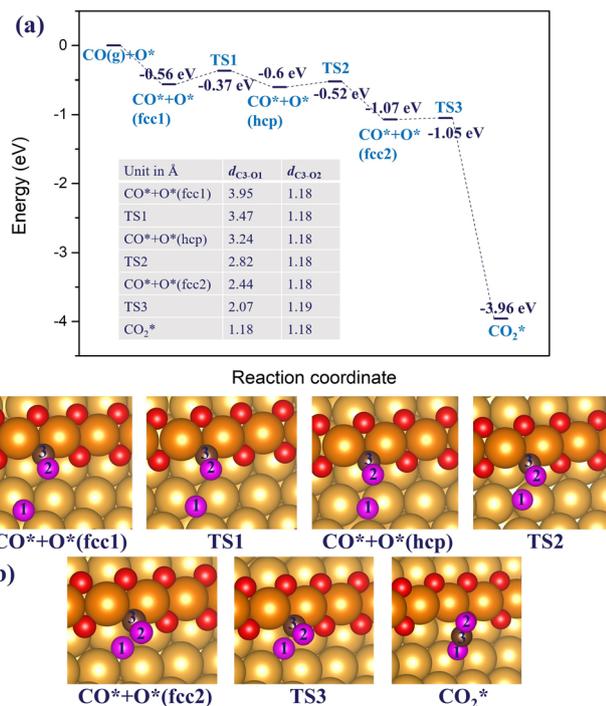

Fig. 8 (a) The reaction energy diagram and (b) the corresponding geometries of CO* reacting with the adsorbed O* atom on the double chain on the Au(221) surface. The labelled C−O bond lengths are listed in a table embedded in the figure (a). Color coding is the same as in Fig. 4.
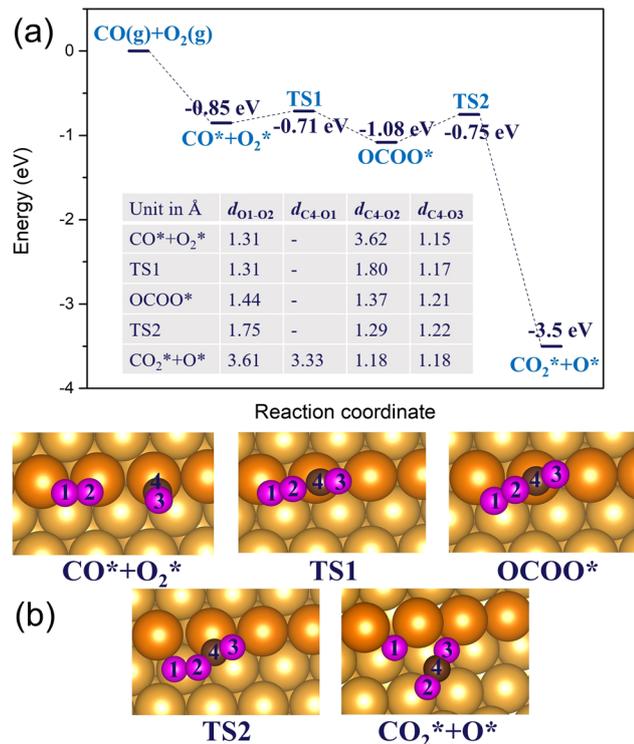
Unit in Å	d_{C3-O1}	d_{C3-O2}
CO*+O*(fcc1)	3.95	1.18
TS1	3.47	1.18
CO*+O*(hcp)	3.24	1.18
TS2	2.82	1.18
CO*+O*(fcc2)	2.44	1.18
TS3	2.07	1.19
CO_2*	1.18	1.18

Fig. 9 (a) The reaction energy diagram and (b) the corresponding geometries of the reaction between the co-adsorbed CO* and O_2* molecules on the regular Au(221) surface. The labelled O–O and C–O bond lengths are listed in a table embedded in the figure (a). Au atoms at the step edge are indicated by an orange color; the remaining Au atoms are shown in gold. O and C atoms of the adsorbates are shown in pink and black, respectively.

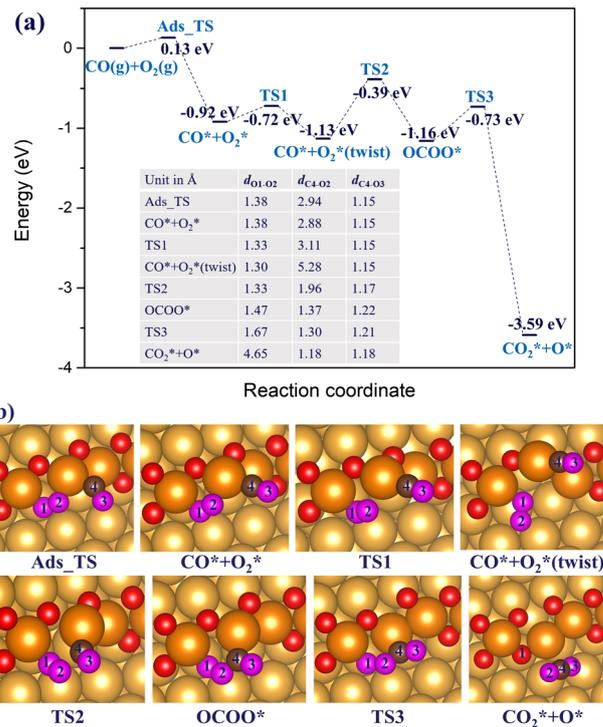
Fig. 10 (a) The reaction energy diagram and (b) the corresponding geometries of the reaction between the co-adsorbed CO* and O_2* molecules on the double chain with two adjacent vacancies on the Au(221) surface. The labelled O–O and C–O bond lengths are listed in a table embedded in the figure (a). Au atoms at the step edge are indicated by an orange color; the remaining Au atoms are shown in gold color. O atoms of the chain structure are shown in red, while O atoms of the adsorbates are shown in pink. C atoms are shown in black.

to that observed in the bulk phase, resulting in a higher reaction rate.

3.2.2 Au(221) surface with a double O chain. Next, we consider CO oxidation by O_2 on a double chain with two-O atom vacancies on a Au(221) surface. CO* and O_2* are initially co-adsorbed at the O-vacant sites, as shown in Fig. 10(b), with the co-adsorption energy of −0.92 eV after structural alignment of the adsorbed molecules which occurred *via* a barrier height of 0.13 eV. Co-adsorption of CO* and O_2* is further stabilized after a structural rearrangement in which a linear fragment O–Au–CO (afterwards denoted as OAuCO) is formed and concomitantly the O_2* molecule is rotated such that now only one O atom (labelled O1) binds at a vacancy site of a chain whereas the other O atom (labelled O2) binds to Au atoms of an underlying terrace. The rearrangement occurs *via* an activation barrier of 0.2 eV and is accompanied by a structural distortion of the Au atoms at the step edge. As such, the step Au atoms appeared twisted. The formed OAuCO unit is stabilized owing to the strong σ-donation from CO* to Au and π-backdonation from Au to C–O bonding. The strengthened Au–C bonding is reflected by the shortening of the Au–C bond length from 1.96 Å in the initial co-adsorption minimum to 1.88 Å in the twisted minimum. The O–O bond length (d_{O1-O2}) decreases from 1.38 Å in the initial co-adsorbed state to 1.30 Å in the twisted

minimum. Because of the change in the orientation of O_2*, the oxygen atom labelled O2 is no longer connected to the Au atoms of a step edge, resulting in less charge transfer to its π* orbital, and a lower degree of activation. The bond length of 1.30 Å is typical of a superoxo (O_2^-) species. This is also consistent with the spin magnetic moment of 0.9 μ_B on the adsorbed O_2* molecule. A quite substantial activation barrier of 0.74 eV is required to form the OCOO* intermediate from the discussed stable minimum. In the transition structure the OAuCO fragment realigns its axis until the distance between CO* and O_2* almost vanishes. Finally, the OCOO* intermediate dissociates to CO_2* and an adsorbed O* atom with an activation barrier of 0.43 eV. The resulting CO_2* has a C–O bond length of 1.18 Å, and desorbs from the surface. Interestingly, comparing the two CO oxidation mechanisms (associative and dissociative) for double chains with two-O atom vacancies on Au(221), we found that the rate-limiting barrier for the association mechanism is comparable in height to the direct O_2* dissociation. This suggests that the two mechanisms may be competing depending on the prevailing temperature and pressure conditions.

Furthermore, we also considered another possible scenario where O_2* adsorbs on a double vacancy of the oxygen chain while the reacting CO* molecule is located at a terrace site adjacent to the step edge. In this case, the co-adsorption energy
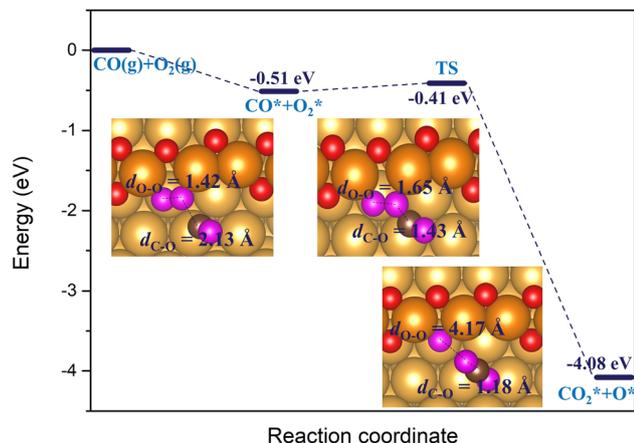
28860 | *Phys. Chem. Chem. Phys.*, 2022, **24**, 28853–28863

This journal is © the Owner Societies 2022

PCCP

Fig. 11 The reaction energy diagram and the corresponding geometries of the reaction between the co-adsorbed CO* and O_2* molecules on the double O chain with two adjacent O vacancies on the Au(221) surface. O_2* adsorbs at a vacancy site while CO* on a terrace site of the surface. Color coding same as in Fig. 10.

of CO* and O_2* reaches up to −0.51 eV on the Au(221) surface with a double O chain and a double O vacancy. As shown in Fig. 11, the co-adsorption complex smoothly changes to a concerted transition state of the OCOO shape with an elongated O–O bond of length 1.65 Å and a forming C–O bond of length 1.43 Å. The activation barrier of this transformation is only 0.1 eV. The transition structure dissociates to form one CO_2* and one O* atom filling the vacancy site of the oxygen chain structure. The reaction barrier is far lower than the 0.74 eV found for an analogous recombination reaction of CO* and O_2* co-adsorbed on the oxygen chain with the adjacent O vacancies. In the latter case, the high barrier is attributed to the formation of the stable OAuCO fragment which is not formed when CO* approaches O_2* from a terrace site. We have identified a number of similar pathways summarized in Fig. S6 (ESI†), which differ slightly from that shown in Fig. 11 by the initial orientation of the interacting CO* and O_2*. The co-adsorption energy varies between −0.51 and −0.63 eV and the activation barrier height from 0.10 to 0.35 eV. Therefore, the results of this computational study suggest that the oxidation of CO will tend to follow an association mechanism in which O_2* is adsorbed at a vacancy site of a double O chain and the CO* molecule is attacking it from a terrace site. Such a mechanism appears to be more plausible than the two mechanisms considered earlier where both CO* and O_2* are co-adsorbed on the oxygen chain or when O_2* dissociates to two O* atoms.

Conclusions

We have investigated the chemisorption of atomic oxygen and the formation of O chains (1D surface gold oxide) along the steps on the Au(221) surface, and compared the reactivity of the regular Au(221) surface and that of the O chain toward catalyzing CO oxidation. We found that O atoms prefer to form a single straight chain along the step of Au(221) with the average

adsorption energy of −0.33 eV per O atom for the infinite single chain. The adsorption strength drops as more O atoms are attached to the chain due to increasing electrostatic repulsion among the O atoms. As the number of O atoms increases further on the surface, eventually an idealized infinite double chain would be formed with an adsorption energy of −0.25 eV per O atom.

Oxygen vacancy formation energies for single and double oxygen vacancies were calculated. The single vacancy requires 0.81 eV to form by releasing one oxygen atom. Two types of double vacancies were investigated, namely, separated and adjacent oxygen vacancies. The latter is easier to form than the former based on their vacancy formation energies.

Oxygen vacancies within the O chain have been shown to be able to bind CO and O_2 stronger than the regular Au(221) surface. CO prefers to adsorb *via* its C end on the regular Au(221), a single oxygen vacancy, and on a double vacancy site with adjacent vacancies with the adsorption energies of around −0.65 eV. On the surface with two separated vacancies CO adsorbs even stronger, with the adsorption energy of −0.76 eV. The O_2 molecule prefers to bind horizontally at all considered types of surface sites with the adsorption energy of −0.22 eV on the regular Au(221) surface, and −0.01 eV, −0.32 eV and −0.34 eV on the O chain with one O vacancy, two adjacent vacancies, and with two separated vacancies, respectively. The increased ability of binding O_2 may lead to a higher activity of chains to CO oxidation than the regular Au(221). To the best of our knowledge, there are no experimental studies on the activity of Au(221) toward CO oxidation, but a recent theoretical work using microkinetic modeling predicted it to have sizable activity at experimentally relevant conditions, even higher than that of Au_{20} clusters.

We investigated the CO oxidation by O_2 on the double O chain with two adjacent O vacancies considering both dissociation and association mechanisms. In the dissociation mechanism, the rate determining step is the dissociation of O_2* for which the barrier height is 0.87 eV on the double O chain with two adjacent vacancies. This value is significantly lower than the 1.84 eV obtained for the regular Au(221) surface, but is still considerably high. In the association mechanism, the formation of an OCOO* intermediate *via* a direct binding of CO* and O_2* is much easier on the regular Au(221) surface with a maximum barrier of 0.33 eV compared to the high reaction barrier of 0.74 eV on the double O chain with two adjacent vacancies. This higher barrier correlates with the strong co-adsorption of CO* and O_2* in the second co-adsorption minimum CO* + O_2* (twist) (Fig. 10(a)). The results of this computational study suggest that both association and dissociation mechanisms may compete on the double chain with two adjacent vacancies depending on the given thermodynamic conditions. However, the energy barrier of an association mechanism drops to only 0.1 eV if the reacting CO* molecule is adsorbed at a terrace site close to O_2* adsorbed at a vacancy site. Therefore, the double oxygen chain formed along the steps on the Au(221) surface is found to enhance the adsorption and activation of O_2, but it possibly hinders the dissociation of OAuCO or OCOO fragments due to the strong interaction of CO* with Au

This journal is © the Owner Societies 2022

Phys. Chem. Chem. Phys., 2022, **24**, 28853–28863 | **28861**

on the oxygen chain. All these findings are consistent with the Sabatier principle which suggests that stronger adsorption of the reactants correlates with a higher activation barrier, whereas too weak adsorption results in the lack of reactivity; hence, some intermediate value is required for optimal performance.

Conflicts of interest

There are no conflicts to declare.

Acknowledgements

References

1 A. Wittstock, J. Biener, J. Erlebacher and M. Bäumer, *Nanoporous gold: from an ancient technology to a high-tech material*, Royal Society of Chemistry, 2012.

2 R. Ciriminna, E. Falletta, C. Della Pina, J. H. Teles and M. Pagliaro, *Angew. Chem., Int. Ed.*, 2016, **55**, 14210–14217.

3 A. Wittstock, V. Zielasek, J. Biener, C. M. Friend and M. Bäumer, *Science*, 2010, **327**, 319–322.

4 K. M. Kosuda, A. Wittstock, C. M. Friend and M. Bäumer, *Angew. Chem., Int. Ed.*, 2012, **51**, 1698–1701.

5 A. Zhang, Y. Chen, Z. Yang, S. Ma, Y. Huang, G. Richter, P. Schützendübe, C. Zhong and Z. Wang, *ACS Appl. Energy Mater.*, 2020, **3**, 336–343.

6 B. S. Takale, X. Feng, Y. Lu, M. Bao, T. Jin, T. Minato and Y. Yamamoto, *J. Am. Chem. Soc.*, 2016, **138**, 10356–10364.

7 T. Barakat, J. C. Rooke, E. Genty, R. Cousin, S. Siffert and B.-L. Su, *Energy Environ. Sci.*, 2013, **6**, 371–391.

8 J. A. Rodriguez, S. D. Senanayake, D. Stacchiola, P. Liu and J. Hrbek, *Acc. Chem. Res.*, 2014, **47**, 773–782.

9 V. Zielasek, B. Jürgens, C. Schulz, J. Biener, M. M. Biener, A. V. Hamza and M. Bäumer, *Angew. Chem., Int. Ed.*, 2006, **45**, 8241–8244.

10 C. Xu, J. Su, X. Xu, P. Liu, H. Zhao, F. Tian and Y. Ding, *J. Am. Chem. Soc.*, 2007, **129**, 42–43.

11 B. Qiao, J.-X. Liang, A. Wang, J. Liu and T. Zhang, *Chin. J. Catal.*, 2016, **37**, 1580–1586.

12 H. Masatake, K. Tetsuhiko, S. Hiroshi and Y. Nobumasa, *Chem. Lett.*, 1987, 405–408.

13 M. Haruta, N. Yamada, T. Kobayashi and S. Iijima, *J. Catal.*, 1989, **115**, 301–309.

14 G. J. Hutchings, *J. Catal.*, 1985, **96**, 292–295.

15 W. Dononelli, L. V. Moskaleva and T. Klüner, *J. Phys. Chem. C*, 2019, **123**, 7818–7830.

16 Z.-P. Liu, P. Hu and A. Alavi, *J. Am. Chem. Soc.*, 2002, **124**, 14770–14779.

17 J. L. Fajin, M. N. D. Cordeiro and J. R. Gomes, *J. Phys. Chem. C*, 2008, **112**, 17291–17302.

18 H. Y. Kim, H. M. Lee and G. Henkelman, *J. Am. Chem. Soc.*, 2012, **134**, 1560–1570.

19 F. R. Negreiros, L. Sementa, G. Barcaro, S. Vajda, E. Aprá and A. Fortunelli, *ACS Catal.*, 2012, **2**, 1860–1864.

20 D. Cheng, H. Xu and A. Fortunelli, *J. Catal.*, 2014, **314**, 47–55.

21 P. Schlexer, D. Widmann, R. J. Behm and G. Pacchioni, *ACS Catal.*, 2018, **8**, 6513–6525.

22 J. M. Gottfried, K. J. Schmidt, S. L. M. Schroeder and K. Christmann, *Surf. Sci.*, 2002, **511**, 65–82.

23 L.-C. Wang, M. L. Personick, S. Karakalos, R. Fushimi, C. M. Friend and R. J. Madix, *J. Catal.*, 2016, **344**, 778–783.

24 M. M. Montemore, M. A. van Spronsen, R. J. Madix and C. M. Friend, *Chem. Rev.*, 2018, **118**, 2816–2862.

25 N. Saliba, D. H. Parker and B. E. Koel, *Surf. Sci.*, 1998, **410**, 270–282.

26 J. Kim, E. Samano and B. E. Koel, *Surf. Sci.*, 2006, **600**, 4622–4632.

27 Y. Xu and M. Mavrikakis, *J. Phys. Chem. B*, 2003, **107**, 9298–9307.

28 R. Pal, L.-M. Wang, Y. Pei, L.-S. Wang and X. C. Zeng, *J. Am. Chem. Soc.*, 2012, **134**, 9438–9445.

29 G. Tomaschun, W. Dononelli, Y. Li, M. Bäumer, T. Klüner and L. V. Moskaleva, *J. Catal.*, 2018, **364**, 216–227.

30 J. L. C. Fajín, M. N. D. S. Cordeiro and J. R. B. Gomes, *J. Phys. Chem. C*, 2007, **111**, 17311–17321.

31 J. L. C. Fajín, M. N. D. S. Cordeiro and J. R. B. Gomes, *Chem. Commun.*, 2011, **47**, 8403–8405.

32 L. V. Moskaleva, S. Röhe, A. Wittstock, V. Zielasek, T. Klüner, K. M. Neyman and M. Bäumer, *Phys. Chem. Chem. Phys.*, 2011, **13**, 4529–4539.

33 M. G. Sensoy and M. M. Montemore, *J. Phys. Chem. C*, 2020, **124**, 8843–8853.

34 J. L. C. Fajín, M. N. D. S. Cordeiro and J. R. B. Gomes, *Surf. Sci.*, 2008, **602**, 424–435.

35 K. Sun, M. Kohyama, S. Tanaka and S. Takeda, *J. Phys. Chem. A*, 2012, **116**, 9568–9573.

36 M. M. Montemore, R. J. Madix and E. Kaxiras, *J. Phys. Chem. C*, 2016, **120**, 16636–16640.

37 L. V. Moskaleva, T. Weiss, T. Klüner and M. Bäumer, *J. Phys. Chem. C*, 2015, **119**, 9215–9226.

38 Y. Li, W. Dononelli, R. Moreira, T. Risse, M. Bäumer, T. Klüner and L. V. Moskaleva, *J. Phys. Chem. C*, 2017, **122**, 5349–5357.

39 F. Hiebel, M. M. Montemore, E. Kaxiras and C. M. Friend, *Surf. Sci.*, 2016, **650**, 5–10.

40 H. Shi and C. Stampfl, *Phys. Rev. B: Condens. Matter Mater. Phys.*, 2007, **76**, 075327.

28862 | *Phys. Chem. Chem. Phys.*, 2022, **24**, 28853–28863

This journal is © the Owner Societies 2022

41 M. Landmann, E. Rauls and W. G. Schmidt, *J. Phys. Chem. C*, 2009, **113**, 5690–5699.

42 X. Deng, B. K. Min, A. Guloy and C. M. Friend, *J. Am. Chem. Soc.*, 2005, **127**, 9267–9270.

43 T. A. Baker, X. Liu and C. M. Friend, *Phys. Chem. Chem. Phys.*, 2011, **13**, 34–46.

44 T. A. Baker, C. M. Friend and E. Kaxiras, *J. Chem. Theory Comput.*, 2010, **6**, 279–287.

45 J. Gong and C. B. Mullins, *Acc. Chem. Res.*, 2009, **42**, 1063–1073.

46 M. Pan, J. Gong, G. Dong and C. B. Mullins, *Acc. Chem. Res.*, 2014, **47**, 750–760.

47 F. Hiebel, S. Karakalos, Y. Xu, C. M. Friend and R. J. Madix, *Top. Catal.*, 2018, **61**, 299–307.

48 F. Xu, M. M. Montemore, C. R. O'Connor, E. Muramoto, M. A. van Spronsen, R. J. Madix and C. M. Friend, *Surf. Sci.*, 2019, **679**, 296–303.

49 C. D. Feldt, T. Gimm, R. Moreira, W. Riedel and T. Risse, *Phys. Chem. Chem. Phys.*, 2021, **23**, 21599–21605.

50 C. D. Feldt, T. Kirschbaum, J. L. Low, W. Riedel and T. Risse, *Catal. Sci. Technol.*, 2022, **12**, 1418–1428.

51 A. M. Venezia, G. Pantaleo, A. Longo, G. Di Carlo, M. P. Casaletto, F. L. Liotta and G. Deganello, *J. Phys. Chem. B*, 2005, **109**, 2821–2827.

52 H. Y. Kim and G. Henkelman, *J. Phys. Chem. Lett.*, 2013, **4**, 216–221.

53 Y.-G. Wang, D. Mei, V.-A. Glezakou, J. Li and R. Rousseau, *Nat. Commun.*, 2015, **6**, 6511.

54 Y. Li, S. Li, M. Bäumer, E. A. Ivanova-Shor and L. V. Moskaleva, *ACS Catal.*, 2020, **10**, 3164–3174.

55 I. X. Green, W. Tang, M. Neurock and J. T. Yates Jr, *Science*, 2011, **333**, 736–739.

56 J. A. Rodriguez, S. Ma, P. Liu, J. Hrbek, J. Evans and M. Perez, *Science*, 2007, **318**, 1757–1760.

57 L. Alves, B. Ballesteros, M. Boronat, J. R. Cabrero-Antonino, P. Concepción, A. Corma, M. A. Correa-Duarte and E. Mendoza, *J. Am. Chem. Soc.*, 2011, **133**, 10251–10261.

58 G. Kresse and J. Furthmüller, *Phys. Rev. B: Condens. Matter Mater. Phys.*, 1996, **54**, 11169.

59 G. Kresse and J. Furthmüller, *Comput. Mater. Sci.*, 1996, **6**, 15–50.

60 P. E. Blöchl, *Phys. Rev. B: Condens. Matter Mater. Phys.*, 1994, **50**, 17953.

61 G. Kresse and D. Joubert, *Phys. Rev. B: Condens. Matter Mater. Phys.*, 1999, **59**, 1758.

62 J. P. Perdew, *Phys. Rev. B: Condens. Matter Mater. Phys.*, 1986, **33**, 8822.

63 J. P. Perdew, K. Burke and M. Ernzerhof, *Phys. Rev. Lett.*, 1996, **77**, 3865.

64 J. Sun, A. Ruzsinszky and J. P. Perdew, *Phys. Rev. Lett.*, 2015, **115**, 036402.

65 H. J. Monkhorst and J. D. Pack, *Phys. Rev. B: Solid State*, 1976, **13**, 5188.

66 M. Methfessel and A. Paxton, *Phys. Rev. B: Condens. Matter Mater. Phys.*, 1989, **40**, 3616.

67 G. Mills, H. Jónsson and G. K. Schenter, *Surf. Sci.*, 1995, **324**, 305–337.

68 G. Henkelman, B. P. Uberuaga and H. Jónsson, *J. Chem. Phys.*, 2000, **113**, 9901–9904.

69 G. Henkelman and H. Jónsson, *J. Chem. Phys.*, 1999, **111**, 7010–7022.

70 G. Blyholder, *J. Phys. Chem.*, 1964, **68**, 2772–2777.

71 H. J. Freund and M. W. Roberts, *Surf. Sci. Rep.*, 1996, **25**, 225–273.

72 W. Dononelli, G. Tomaschun, T. Klüner and L. V. Moskaleva, *ACS Catal.*, 2019, **9**, 5204–5216.

73 J. D. Lee, J. B. Miller, A. V. Shneidman, L. Sun, J. F. Weaver, J. Aizenberg, J. Biener, J. A. Boscoboinik, A. C. Foucher, A. I. Frenkel, J. E. S. van der Hoeven, B. Kozinsky, N. Marcella, M. M. Montemore, H. T. Ngan, C. R. O'Connor, C. J. Owen, D. J. Stacchiola, E. A. Stach, R. J. Madix, P. Sautet and C. M. Friend, *Chem. Rev.*, 2022, **122**, 8758–8808.

74 J. Biener, M. M. Biener, R. J. Madix and C. M. Friend, *ACS Catal.*, 2015, **5**, 6263–6270.

This journal is © the Owner Societies 2022

Phys. Chem. Chem. Phys., 2022, **24**, 28853–28863 | **28863**